ADVANCED THERAPEUTICS
www.advtherap.com

Does Encapsulation of π-Conjugated Polymer Nanoparticles within Biodegradable PEG–PLGA Matrices Mitigate Photoinduced Free Radical Production and Phototoxicity?

*Paola Modicano, Marie-Luise Trutschel, Thüong Phan-Xuan, Bruno F. E. Matarèse, Laura Urbano, Mark Green, Karsten Mäder, and Lea Ann Dailey**

Lipophilic π-conjugated polymers (CPs) encapsulated within self-assembling diblock copolymer poly(ethylene glycol) methyl ether-*block*-poly(lactide-*co*-glycolide) (PEG–PLGA) nanoparticles, are interesting candidates for photodynamic and photothermal therapies. Upon irradiation, CPs generate reactive oxygen species (ROS), which may either cause local phototoxicity or could be exploited for photodynamic therapy. The propensity of the PEG–PLGA matrix to scavenge ROS has never been investigated. Here the ability of two PEG–PLGA structures ($PEG_{2\ kDa}$–$PLGA_{4.5\ kDa}$ vs $PEG_{5\ kDa}$–$PLGA_{55\ kDa}$) to mitigate the release of ROS generated by four different CPs (PFO, F8BT, CN-PPV, and PCPDTBT) following irradiation (5 J cm^{-2}) at 385, 455, and 656 nm is studied. The molar content of the PEG–PLGA matrix, rather than the molecular weight or composition, appeared to be the most influential factor, i.e., lower molar concentrations of the matrix polymer are associated with significant increases in phototoxicity. Multivariate analysis reveals that the combination of CP photophysical properties and nanoparticle matrix properties are important for understanding CP nanoparticle-induced phototoxicity.

1. Introduction

π-conjugated polymers (CPs) are an interesting class of macromolecules with potential applications in optical and photoacoustic imaging, photothermal (PTT), and photodynamic therapy (PDT).[1–8] Their unique structure combines excellent light harvesting properties with a large delocalized electronic structure in the polymer backbone.[8,9] Excitons are able to migrate along the polymer backbone or hop between chains with ease, resulting in semiconducting properties.[10,11] Upon light irradiation, electrons in the CP backbone are elevated from their ground state (S0) to the excited state (S2) before falling into the lowest vibrational level of the excited state (S1) via internal relaxation[12] (**Figure 1**). At this point, different processes can occur, which can be exploited for various biomedical applications: 1) fluorescence: the electron relaxes back into the ground state while concurrently emitting a photon with a Stokes shift in wavelength;[12] 2) heat dissipation: the electron returns to the ground state while trans-

P. Modicano, M.-L. Trutschel, K. Mäder
Institute of Pharmacy
Martin-Luther-Universität Halle-Wittenberg
Kurt-Mothes Str. 3, 06120 Halle (Saale), Germany

T. Phan-Xuan
Vienna Doctoral School of Pharmaceutical
Nutritional and Sport Sciences (PhaNuSpo)
University of Vienna
Josef-Holaubek-Platz 2, Vienna 1090, Austria

B. F. E. Matarèse
Department of Haematology
Cambridge Biomedical Campus
University of Cambridge
Electrical Engineering Division
University of Cambridge
Cambridge CB2 1TN, UK

L. Urbano
Department of Clinical
Pharmaceutical and Biological Science
University of Hertfordshire
Hatfield, Hertfordshire AL10 9AB, UK

M. Green
Department of Physics
King's College London
Strand Campus
London WC2R 2LS, UK

L. A. Dailey
Department of Pharmaceutical Sciences
University of Vienna
Josef-Holaubek-Platz 2, Vienna 1090, Austria
E-mail: leaann.dailey@univie.ac.at

The ORCID identification number(s) for the author(s) of this article can be found under https://doi.org/10.1002/adtp.202400190

© 2024 The Author(s). Advanced Therapeutics published by Wiley-VCH GmbH. This is an open access article under the terms of the Creative Commons Attribution-NonCommercial-NoDerivs License, which permits use and distribution in any medium, provided the original work is properly cited, the use is non-commercial and no modifications or adaptations are made.

DOI: 10.1002/adtp.202400190

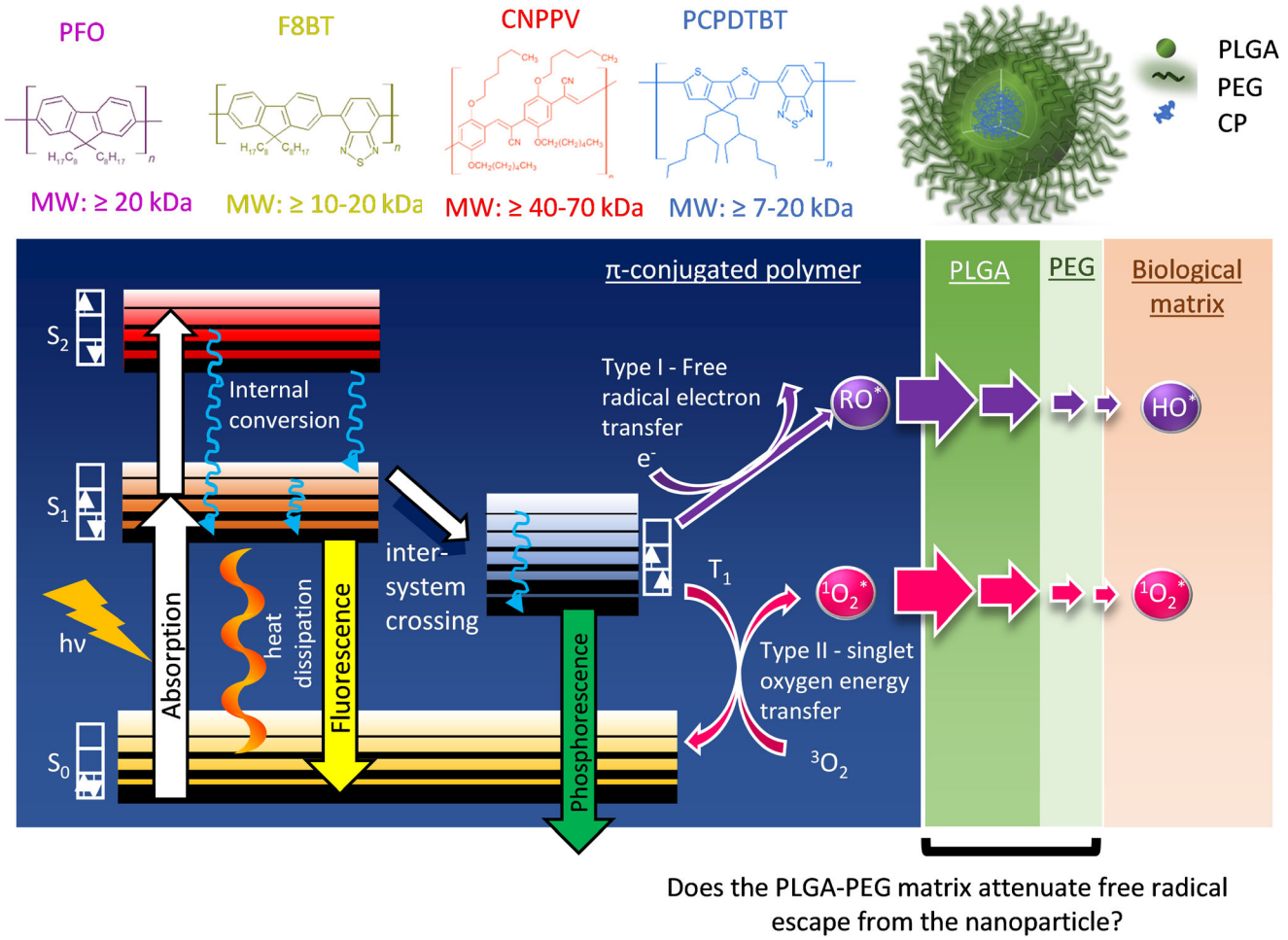

Figure 1. A–D) Chemical structure of CPs chosen for the study and E) representation of CPN structure following self-assembly in water. F) Simplified illustration of a Jablonski diagram showing different transitions between energy states and highlighting pathways for the generation of free radicals (type I reactions) and singlet oxygen $^1O_2$ (type II reactions). Modified from Meng et al.[13]

ferring energy to the surrounding environment in the form of heat; or 3) intersystem crossing from the singlet to triplet state, a process that can be accompanied by either a photon emission (phosphorescence)[12] or the generation of free radicals (type I reaction) as well as singlet oxygen $^1O_2$ (type II reaction).[13] CPs which exhibit pronounced fluorescence and phosphorescence can be useful as contrast agents for optical imaging.[1] In contrast, CPs which primarily convert energy into thermal relaxation and heat generation are much better suited for PTT.[1] It also follows that CPs with the ability to generate higher levels of free radicals or singlet oxygen are suitable as photosensitizers in PDT.[1,13]

It is important to consider that fluorescence emission, thermal relaxation, intersystem crossing, and radical/singlet oxygen production are processes that occur simultaneously. The balance between these different processes is highly dependent on the individual CP structure.[3,13–15] Some CPs therefore may have more favorable properties for fluorescence imaging, photoacoustic imaging, PTT[14] or PDT, while other CPs may possess attributes making them suitable for multiple functions.[1,3,6,8] It should also be remembered that some of the afore mentioned attributes may be detrimental within the context of the proposed biomedical application. For example, CPs designed as imaging contrast agents may induce substantial amounts of reactive oxygen species (ROS) at off-target sites in the body thereby causing nonspecific phototoxicity to healthy tissues.[1] This form of photosensitization has been observed for certain drug compounds with excellent light harvesting properties. While photoallergy induced by systemically administered agents is rather rare, documented clinical cases have been reported.[16,17] This potential for off-target photoallergy has not yet been evaluated for systemically administered CP systems.

Another important aspect to consider is how the CP formulation may influence the balance between fluorescence emission, thermal relaxation, intersystem crossing, and ROS production/release. As highly hydrophobic macromolecules, CPs are rarely colloidally stable in aqueous media without stabilizing agents.[1,8,9] We have investigated the strategy of encapsulating a series of different CPs within either the liquid core of medium-chain triglycerides of lipid nanocapsules[18] or within a matrix of the biodegradable copolymer, poly(ethylene glycol) methyl ether-*block*-poly(lactide-*co*-glycolide) (PEG–PLGA) to ensure colloidal stability and improve biocompatibility.[19–25] Am-

© 2024 The Author(s). Advanced Therapeutics published by Wiley-VCH GmbH

phiphilic PEG–PLGA chains self-assemble in aqueous solutions to form polymer micelles with a hydrophobic core able to encapsulate CPs over a wide concentration range.[20,21,23] The hydrophilic PEG component decorates the surface of the polymer micelle providing steric stabilization, colloidal stability, and the possibility of further surface functionalization.[26] The resulting π-conjugated polymer nanoparticles (CPNs) produced with PEG–PLGA have been shown to exhibit the required attributes for parenteral administration, in terms of size, colloidal stability, purity, and sterility.[22,24] We have observed that the type of PEG–PLGA matrix polymer chosen for CP encapsulation has an impact on CP properties such as fluorescence and photoacoustic signal intensity.[24] Furthermore, using thermal lens spectrometry to investigate CPNs containing the NIR emitting poly[2,6-(4,4-bis-(2-ethylhexyl)-4H-cyclopenta[2,1-b;3,4-b′]dithiophene)-alt-4,7(2,1,3-benzothiadiazole)] (PCPDTBT) we determined that both the type of PEG–PLGA matrix and the CPN production method (i.e., bulk precipitation vs microfluidics) influences the fraction of absorbed energy converted to heat.[27] For example, samples prepared by microfluidics containing the same PCPDTBT content, but differing PEG–PLGA matrices showed a high fraction of nonradiative thermal relaxation for $PEG_{5\,kDa}$–$PLGA_{55\,kDa}$ (≈0.8) in contrast to the low thermal relaxation fraction observed for $PEG_{2\,kDa}$–$PLGA_{15\,kDa}$ (≈0.05) matrices. Samples prepared by bulk precipitation, in contrast to microfluidics, showed an intermediate fraction of nonradiative thermal relaxation regardless of PEG–PLGA matrix (≈0.6).[27]

When considering the generation and release kinetics of photoinduced ROS, the chemical structure of the PEG–PLGA matrix will also be important.[28] The PEG–PLGA matrix may act as a reaction partner or scavenger for generated ROS. Furthermore, the structure influences the hydrophobicity of the NP and thus the oxygen distribution within the matrix due to the lipophilicity of the oxygen. It is hypothesized that oxygen permeability will be lower in the more lipophilic PEG–PLGA matrices.[29] The release kinetics of oxygen will also depend on the lactide to glycolide ratio,[30] as well as the molecular weight of the PEG coating. In previous work, it has been observed that PEG facilitates singlet oxygen release.[30]

To test the impact of the PEG–PLGA matrix on CPN phototoxicity,[31] we investigate two PEG–PLGA structures: low molecular weight $PEG_{2\,kDa}$–$PLGA_{4.5\,kDa}$ (abbreviated as P6.5k) and high molecular weight $PEG_{5\,kDa}$–$PLGA_{55\,kDa}$ (abbreviated as P60k). Four different CPs (PFO, F8BT, CN-PPV, and PCPDTBT) were encapsulated the respective PEG–PLGA matrices (5% CP w/w) and ROS release as well as cellular phototoxicity was evaluated following irradiation (5 J cm^{-2}) at 385, 455, and 656 nm. The four CPs were chosen because three of the CPs (PFO, F8BT, and CN-PPV) are characterized by high photoluminescence quantum yields (PLQYs), higher intracellular ROS production, and low nonradiative thermal relaxation.[32] As such, these materials have been proposed to be classified as Group 1 CPs, which may be more suited to PDT therapy.[32] PCPDTBT, in contrast, which is characterized by a low PLQY and a much higher nonradiative thermal relaxation[27] would be classified by Feyen et al. as a Group 2 CP,[32] which would be more suited to PTT. Three irradiation wavelengths were used for photostimulation of the systems to characterize not only the behavior of the CPNs at their ideal excitation wavelengths but also to assess their behavior at nonpeak or off-target wavelengths. The hypothesized behavior of the four different CPs at each wavelength (based on literature reports of the absorbance spectra, photoluminescence and nonradiative thermal relaxation[20–25,27]) is depicted in **Figure 2**. We further hypothesize that the higher molecular weight $PEG_{5\,kDa}$–$PLGA_{55\,kDa}$ will act as a more effective ROS scavenger, due to the combination of the higher molecular weight of the matrix polymer and longer PEG chains.[29,30] To our knowledge, information about the effects of both off-target irradiation and the influence of excipients on ROS release is rarely reported but may be informative in the course of safety and efficacy testing of novel PDT and PTT agents.

2. Results and Discussion

2.1. Physicochemical Characterization and Cellular Uptake of CPN

Only one CP, namely, CN-PPV, has sufficient electronegativity to be colloidally stable at higher concentrations without the use of a stabilizing agent. Therefore, CN-PPV (100%) nanoparticles were used as a reference material throughout the study. Incorporation of 5% (w/w) CP within the P6.5k PEG–PLGA matrix led to a significant increase in hydrodynamic diameter compared to blank nanoparticles (from ≈40 to 80–120 nm; $p < 0.001$). In contrast, the size of the P60k nanoparticles was not influenced by CP incorporation (**Figure 3A**). The key reason why the lower molecular weight polymer (P6.5k PEG–PLGA) requires more molecules to stabilize the CP, while the higher molecular weight polymer (P60k PEG–PLGA) can incorporate CPs without significantly altering the particle size, relates to differences in chain length, packing density, and flexibility of the two polymers, a phenomenon we have observed in previous studies.[23] As expected, the zeta potential of PEG–PLGA CPNs was less electronegative than the CN-PPV 100% system, due to the presence of the PEG decorating the particle surface (Figure 3B). The combination of surface pegylation with a low zeta potential typically leads to reduced cellular uptake in cells.[33] The cellular internalization of CPNs was generally <2% in the 3T3 fibroblasts (Figure 3C), which is expected, given that fibroblasts are nonphagocytic cells with only a limited endocytic capability.[33,34] The low cellular uptake may indicate that photoinduced cytotoxicity measured in subsequent studies could result primarily from extracellular ROS generation in the medium (Dulbecco's phosphate buffered saline; DPBS) rather than depending on intracellular ROS generation.[35]

2.2. Optical Attributes, ROS Generation/Release, and Phototoxicity of PFO CPNs

To study the impact of both CP type and PEG–PLGA matrix effect on the phototoxicity of the four CPN systems, the optical properties and phototoxicity data of each individual CP were grouped into a single figure. PFO exhibits a narrow absorbance peak between 300 and 400 nm (**Figure 4A**) with a large molar extinction coefficient (7–8 × 10^5 M^{-1} cm^{-1}; **Table 1**), indicating excellent light harvesting properties in the UV spectrum. PFO has a

© 2024 The Author(s). Advanced Therapeutics published by Wiley-VCH GmbH

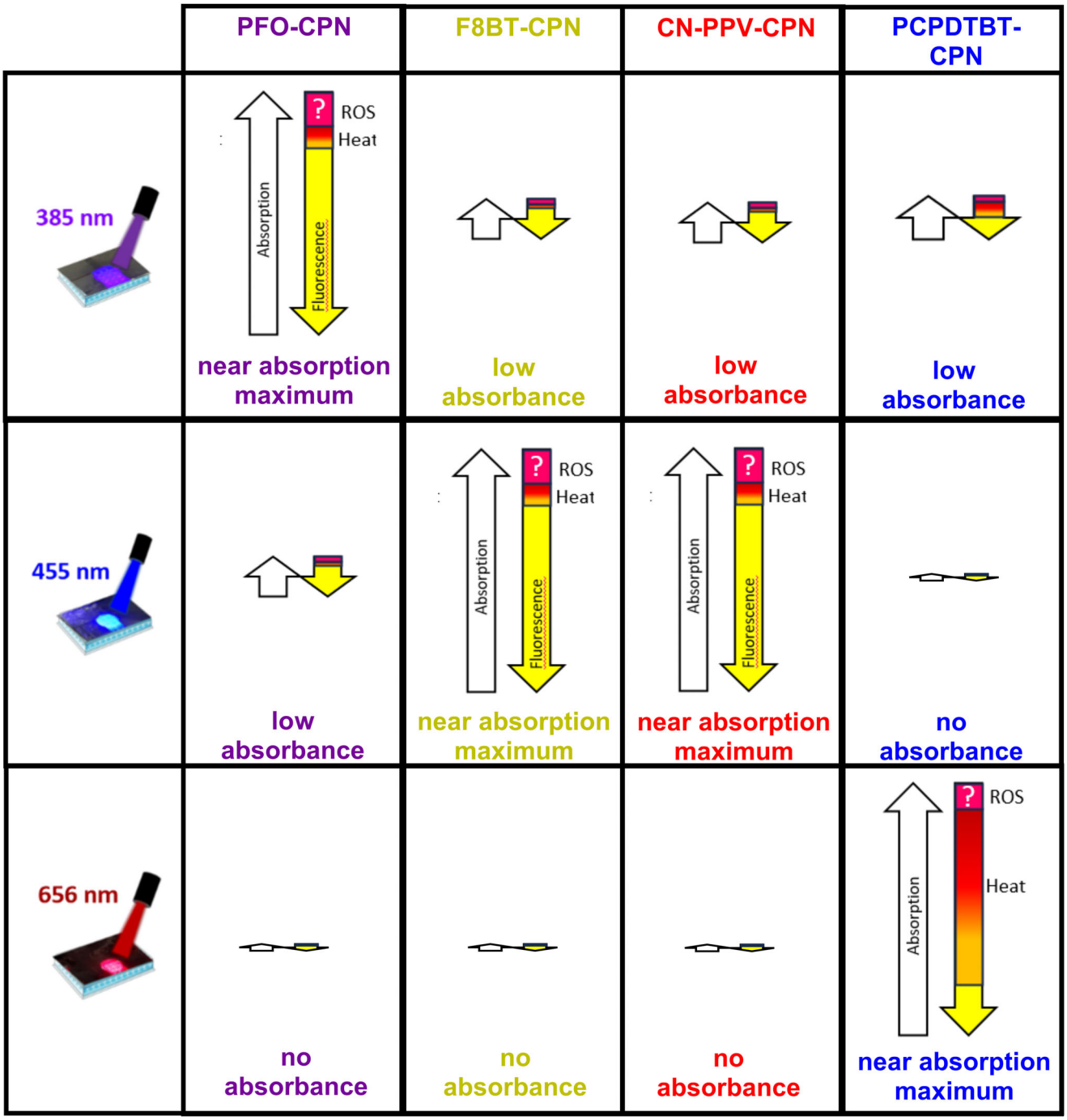

Figure 2. Summary of hypothesized behavior of the four CPNs studied here following illumination at 385, 455, and 656 nm.

distinctive trimodal emission spectrum, which is red-shifted following encapsulation within a PEG–PLGA matrix (Figure 4B). This encapsulation reduces the photoluminescent quantum yield (PLQY%) of PFO by ≈60–70%, although compared to other CPs, the PFO PLQY% is still remarkably high (30–40%; Figure 4C), indicating that a substantial amount of harvested light is converted to photoluminescent emission.

Irradiation-induced ROS generation/release was measured by two methods, electron paramagnetic resonance (EPR) and ascorbic acid (AA) depletion. Both methods, although varying in sensitivity, have the advantage that they are not reliant on quantification of a fluorescence probe, which was determined in pilot studies to be problematic due to a combination of fluorescence overlap with the CPN and photobleaching (see Figures S5–S10, Supporting Information). The EPR spin trap, 5,5-dimethyl-1-pyrrolin-N-oxid (DMPO), is sensitive to radicals with a short lifetime, with affinities to the following species: NO• < O2• < HOO• < HS• < H3C• < HO•.[36] Therefore, it is ideal to de-

© 2024 The Author(s). Advanced Therapeutics published by Wiley-VCH GmbH

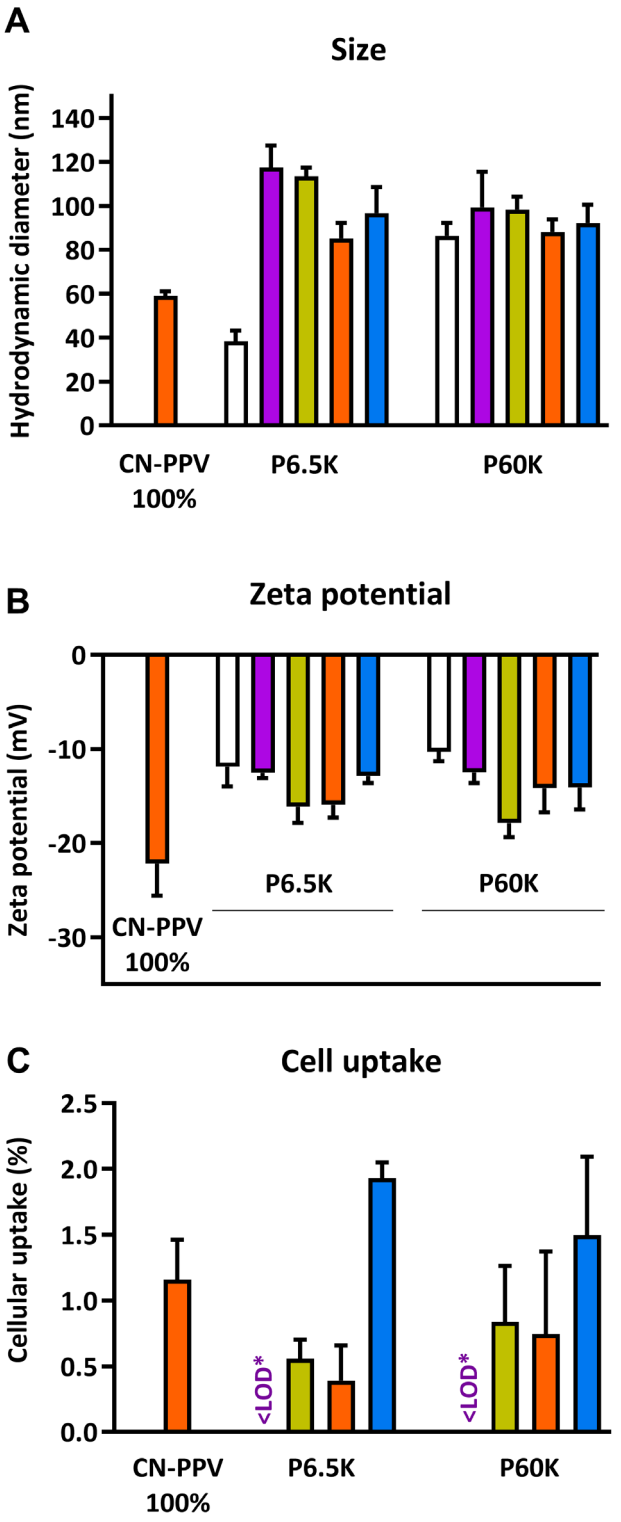

Figure 3. A) CPN size, B) zeta potential, and C) cellular uptake in 3T3 fibroblasts following 1 h incubation at 37 °C in Dulbecco's phosphate buffered saline (DPBS). (A,B) Values represent the mean ± standard deviation from $n = 3$ CPN batches, whereas cell uptake data (C) represent the mean ± standard deviation from $n = 12$ CPN batches tested on 12 cell passage numbers.

tect short-lived hydroxyl radicals (type I reactions; Figure 1). Additionally, singlet oxygen can react in a photosensitizing reaction with DMPO forming DMPO-OH.[36] Therefore, a separation of DMPO-OH from hydroxyl radicals and singlet oxygen is not possible. The oxidation of AA, in contrast, is induced by a broad range of both short- and long-lived ROS.[37]

As hypothesized, short-lived radical formation was highest following PFO CPN irradiation at 385 nm (near the maximum excitation wavelength of PFO), although measurable DMPO-OH quantities were also observed following irradiation at 455 nm, but not with the 656 nm laser (Figure 4D). AA depletion (Figure 4E) was also highest following irradiation at 385 nm and the type of PEG–PLGA matrix did not influence the results. Unexpectedly, irradiation at 656 nm induced a 10–15% reduction in AA content, which was significant compared to non-irradiated samples. Since hydroxyl radical formation was not detectable under these irradiation conditions (Figure 4D), the oxidation of AA is likely due to other mechanisms, e.g., AA oxidation by superoxide radicals. In general, the presence of biological reductants such as AA is linked with increased production of $^1O_2$-derived HO·, which is why AA depletion is typically higher than DMPO-OH formation.[38]

Due to the higher levels of radicals generated via irradiation at 385 nm, it was hypothesized that the cell viability of 3T3 fibroblasts would be reduced under these conditions. Surprisingly, this was not observed (Figure 4F, upper graph). Although minor reductions in cell viability were recorded for all irradiated samples, they were not significantly lower than the cell viability of non-irradiated samples or PEG–PLGA nanoparticles without CP. One possible explanation for this observation is that the species and composition of ROS generated by PFO may have a lower inherent biological reactivity compared to other systems. Indeed, in a consensus statement published by Murphy et al. the authors stress that oxidative damage in cells can take many forms and evaluation of damage from selected ROS in isolation is highly complex.[39] In addition, the inherent antioxidant defense system of cells (e.g., intracellular production of glutathione and other antioxidants),[35,40] is upregulated in response to oxidative stress in the environment and may be more effective against certain types of ROS than others.[35,39]

2.3. Optical Attributes, ROS Generation/Release, and Phototoxicity of F8BT CPNs

F8BT exhibits an absorbance peak between ≈350 and 500 nm (**Figure 5A**) with a molar extinction coefficient (3–4 × 10^5 M^{-1} cm^{-1}; Table 1), which indicates that this CP exhibits excellent light harvesting properties in the UV to visible range of the radiation spectrum. Interestingly, encapsulation in a PEG–PLGA matrix does not induce a red-shift in the F8BT emission profile (Figure 5B) but reduces the PLQY% of F8BT by ≈80% compared to tetrahydrofuran (THF) (CPN PLQY% ≈13–17%; Figure 5C). Laser irradiation at both 385 and 455 nm results in significant amounts of DMPO-OH generated/released (Figure 5D), as well as significant decreases in AA content (Figure 5E), while excitation at 656 nm does not result in DMPO-OH formation or AA depletion. A significant reduction in 3T3 fibroblast viability is observed at both 385 and 455 nm. Interestingly, loss of cell viability

© 2024 The Author(s). Advanced Therapeutics published by Wiley-VCH GmbH

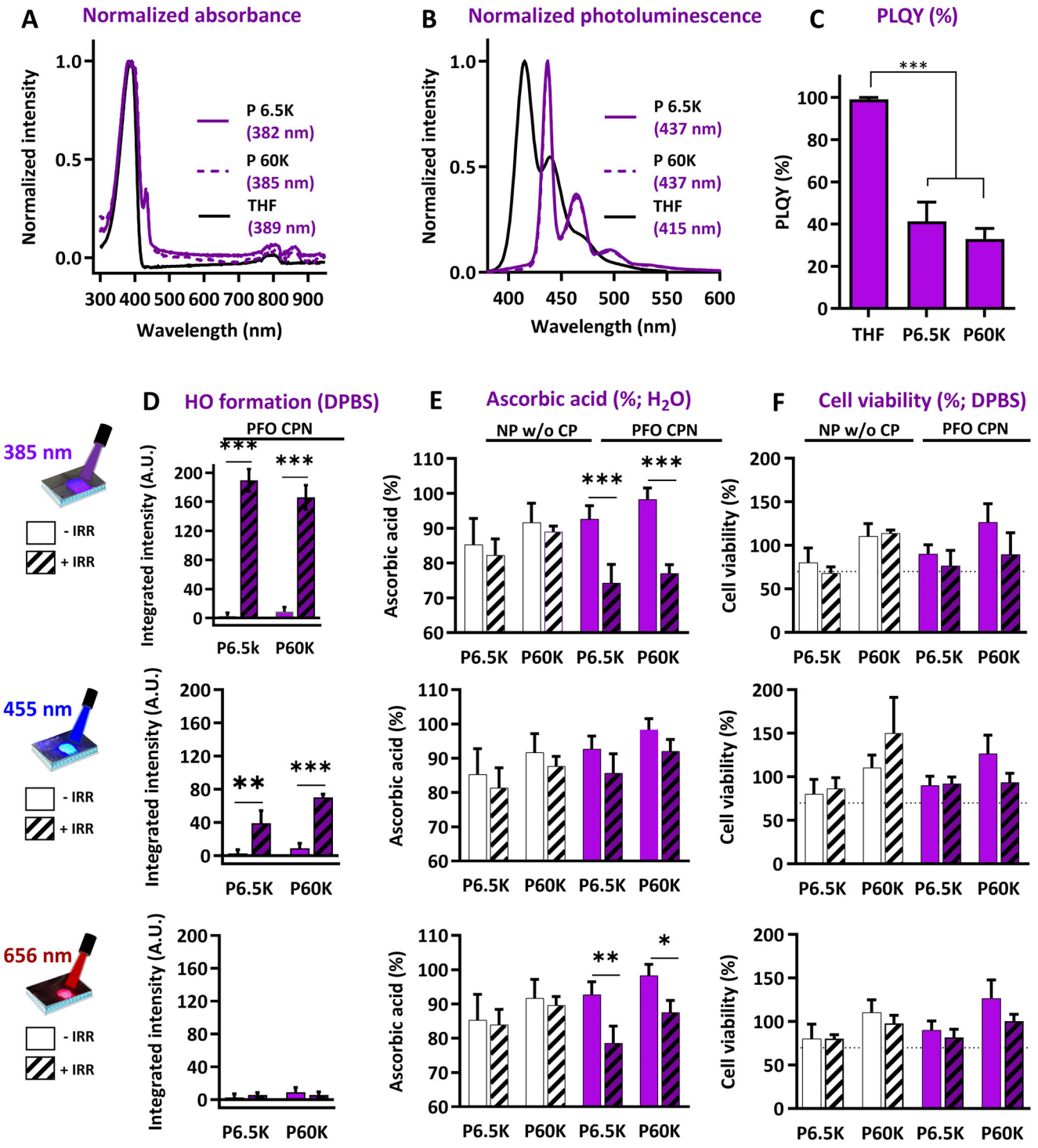

Figure 4. Optical attributes, ROS generation, and phototoxicity of PFO CPNs A) absorbance spectrum, B) emission spectrum, C) PLQY%, D) ROS generation/release of PFO CPNs in DPBS (30 μg mL^{-1}) measured by EPR, E) ROS generation/release as measured by ascorbic acid (AA) depletion, and F) phototoxicity in 3T3 fibroblasts. (A,B) Spectra are representative of at least $n = 3$ individual samples. (C) Values represent the mean ± standard deviation from $n = 3$ CPN batches, whereas phototoxicity data represent the mean ± standard deviation from $n = 3$ CPN batches tested on three cell passage numbers. *($p < 0.05$), **($p < 0.01$), ***($p < 0.001$), ****($p < 0.0001$), indicate significant difference.

© 2024 The Author(s). Advanced Therapeutics published by Wiley-VCH GmbH

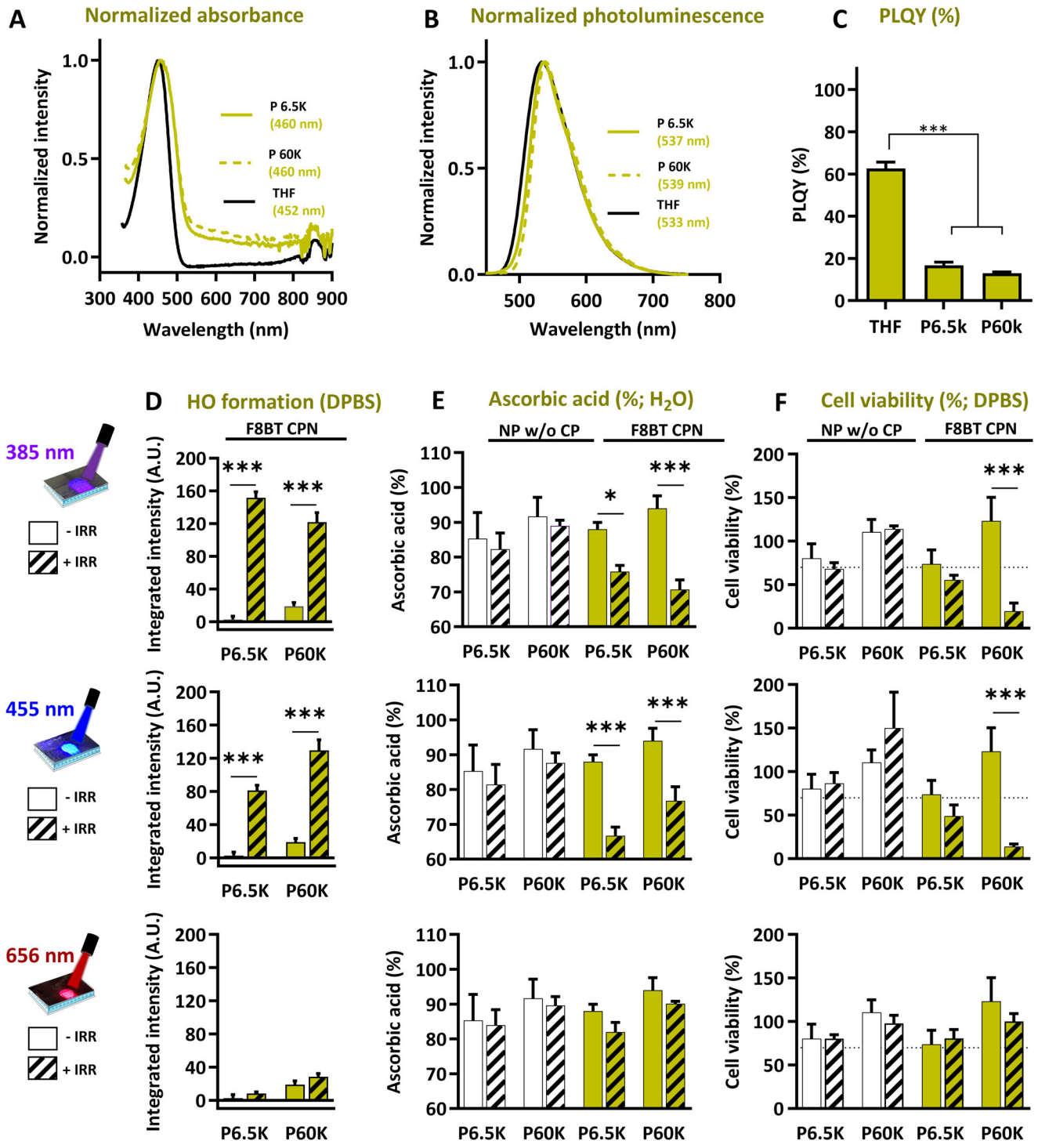

Figure 5. Optical attributes, ROS generation, and phototoxicity of F8BT CPNs. A) Absorbance spectrum, B) emission spectrum, C) PLQY%, D) ROS generation/release in DPBS (30 μg mL^{-1}) measured by EPR, E) ROS generation/release as measured by AA depletion, and F) phototoxicity in 3T3 fibroblasts. Spectra in A and B are representative of at least $n = 3$ individual samples. Values in (C) represent the mean ± standard deviation from $n = 3$ CPN batches, whereas phototoxicity data represent the mean ± standard deviation from $n = 3$ CPN batches tested on three cell passage numbers. *($p < 0.05$), **($p < 0.01$), ***($p < 0.001$), ****($p < 0.0001$), indicate significant difference.

© 2024 The Author(s). Advanced Therapeutics published by Wiley-VCH GmbH

Table 1. Estimated molar absorption coefficients of the CPN calculated from the median reported molecular weight of the polymer and the slope of the calibration curve. Values for the photothermal conversion efficiency (ηPT%) are taken from literature reports.

CP	λ [nm]	ϵ [$\times 10^5$ M^{-1} cm^{-1}]		Photothermal conversion efficiency (ηPT%) of the CP@peak illumination
		P6.5k	P60k	
PFO	350	7.7	8.2	8.1[32]
F8BT	410	4.3	4.2	9.8[32]
CN-PPV	465	8.3	7.9	5.4[32]
PCPDTBT	700	3.9	3.6	≈60[27]

is more pronounced for the high molecular weight P60k PEG–PLGA matrix compared to the P6.5k matrix (Figure 5F).

2.4. Optical Attributes, ROS Generation/Release, and Phototoxicity of CN-PPV CPNs

The pronounced electronegativity of the cyano groups within the backbone of the CN-PPV polymer combined with the relative flexibility of polymer chain provides the CN-PPV polymer with a certain degree of amphiphilicity. Thus, when CN-PPV is dissolved in an organic solvent and then injected into water, this CP forms colloidally stable nanoparticles without the need for an amphiphilic matrix polymer or surfactant stabilizer to ensure colloidal stability.[21] This unique attribute allowed us to compare the behavior of CN-PPV encapsulated within a PEG–PLGA matrix to nanoparticles comprised of 100% CN-PPV and determine the extent of the matrix effect on phototoxicity. Both precipitation (100% CN-PPV nanoparticles) and encapsulation of CN-PPV within a PEG–PLGA matrix induce a red-shift of CN-PPV absorbance, as well as emission, compared to the THF solution (**Figure** 6A,B). Intriguingly, neither precipitation nor encapsulation reduced the PLQY% of CN-PPV compared to THF but rather showed a marginal increase (Figure 6C). Similar to F8BT, laser irradiation at both 385 and 455 nm induced significant amounts of DMPO-OH formation (Figure 6D) and the presence of a P60k PEG–PLGA matrix showed only a minor inhibition of radical release into the bulk fluid compared to 100% CN-PPV nanoparticles. However, despite measurable DMPO-OH formation after irradiation at 385 and 455 nm, neither the 100% CN-PPV nanoparticles nor the CN-PPV CPNs caused AA depletion (Figure 6E), which was surprising, especially since 100% CN-PPV nanoparticles were highly cytotoxic after irradiation at these two wavelengths (Figure 6F). It was also interesting to note that both PEG–PLGA matrix CPNs substantially reduce cytotoxicity at 455 nm compared to CN-PPV 100% systems, indicating an influence of the matrix on phototoxicity.

2.5. Optical Attributes, ROS Generation/Release, and Phototoxicity of PCPDTBT CPNs

Of all the CPs investigated in this study, PCPDTBT is the only CP suitable for in vivo imaging and PTT applications because both its absorbance and emission maxima appear in the near infrared range or tissue transparency window of the radiation spectrum.[37,38] PCPDTBT CPNs exhibit a bimodal absorbance profile (peaks at ≈400 nm and 660/700 nm) with a minor blue-shift compared to the CP in THF (**Figure** 7A). Encapsulation in a PEG–PLGA matrix results in a pronounced red-shift of the emission profile compared to CP in THF (Figure 7B) and also dramatically decreases the PLQY% by ≈22–55-fold compared to THF (PLQY% ≈0.02–0.05%; Figure 7C). Laser irradiation at all three wavelengths induced measurable amounts of DMPO-OH but only in the P60k matrix systems (Figure 7D). It is possible that other radicals are formed which cannot be trapped by DMPO. The kinetics of spin trapping are quite complex also due different stabilities of spin adducts. Further details about spin trapping can be found in a recent publication about radical detection in polysorbates.[41] AA depletion was observed in systems irradiated at 385 and 656 nm (Figure 7E), which corresponded to the two peaks of the PCPDTBT absorbance spectrum. However, no apparent correlation between DMPO-OH generation and AA depletion could be observed. AA can also be decomposed in the presence of ion traces (e.g., copper, iron) or oxidized by superoxide anion radicals, which cannot be trapped by DMPO. There was also no apparent relationship between AA depletion and the fibroblast cell viability following exposure to PCPDTBT CPNs and irradiation at all three wavelengths (Figure 7F), even though CPN uptake in cells was roughly 25–50% higher for this CPN class.

2.6. Analysis of Combined Results

The primary question addressed in this study was whether the type of PEG–PLGA matrix (P6.5k vs P60k) impacts ROS release and phototoxicity. The release of short-lived free radicals (as measured by EPR; **Figure** 8A) showed a trend toward a lower release for the P6.5k PEG–PLGA matrices, especially in the PCPDTBT group, compared to the P60k matrix, although the overall differences between the two sample sets were not significant (p = 0.6311). The data set for long-lived radicals (as measured by AA depletion) showed no indications of a matrix-effect (Figure 8B). In contrast, phototoxicity was significantly higher for systems with P60k PEG–PLGA matrices (unpaired Student's t-test; p = 0.0019). Although our initial hypothesis postulated that the larger molecular weight matrix polymer (P60k) would act as a more effective ROS scavenger, we did not take into consideration differences between mass and molar concentrations of the matrix polymer in the system. In standard CPN preparations, the matrix polymer is present at a concentration of 2 mg mL^{-1}, which equates to a molar concentration of ≈0.3 M for the low molecular weight PEG–PLGA polymer (P6.5k) and a tenfold lower molar concentration of 0.03 M for the high molecular weight polymer (P60k). Of this, the amount of PEG present in the P6.5k systems is ≈62% (≈0.2 M PEG), while the amount of PEG in the P60k systems is only 8% (≈0.0025 M PEG). Thus, the lower molar concentrations of the matrix polymer in the P60k systems may be one contributing factor to the higher cytotoxicity observed with this choice of matrix polymer.

We further employed single parameter (Figure S11, Supporting Information) and multivariate regression analysis (**Figure** 9A–D) to explore the key attributes, which contributed the most

© 2024 The Author(s). Advanced Therapeutics published by Wiley-VCH GmbH

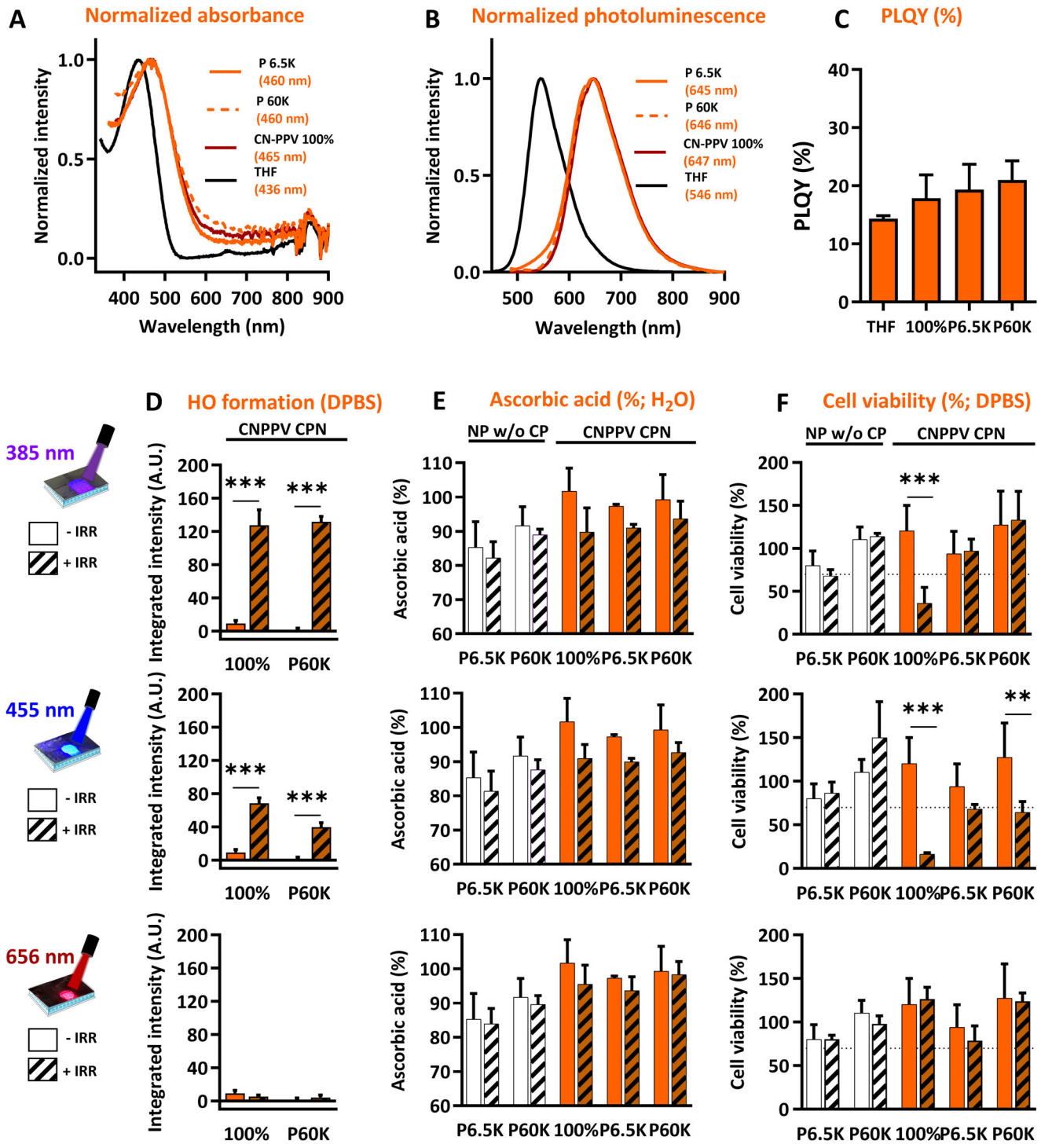

Figure 6. Optical attributes, ROS generation, and phototoxicity of precipitated CN-PPV (100%) and CN-PPV CPNs. A) Absorbance spectrum, B) emission spectrum, C) PLQY%, D) ROS generation/release in DPBS (30 μg mL^{-1}) measured by EPR, E) ROS generation/release as measured by AA depletion, and F) phototoxicity in 3T3 fibroblasts. (A,B) Spectra are representative of at least $n = 3$ individual samples. (C) Values represent the mean ± standard deviation from $n = 3$ CPN batches, whereas phototoxicity data represent the mean ± standard deviation from $n = 3$ CPN batches tested on three cell passage numbers. *($p < 0.05$), **($p < 0.01$), ***($p < 0.001$), ****($p < 0.0001$), indicate significant difference.

© 2024 The Author(s). Advanced Therapeutics published by Wiley-VCH GmbH

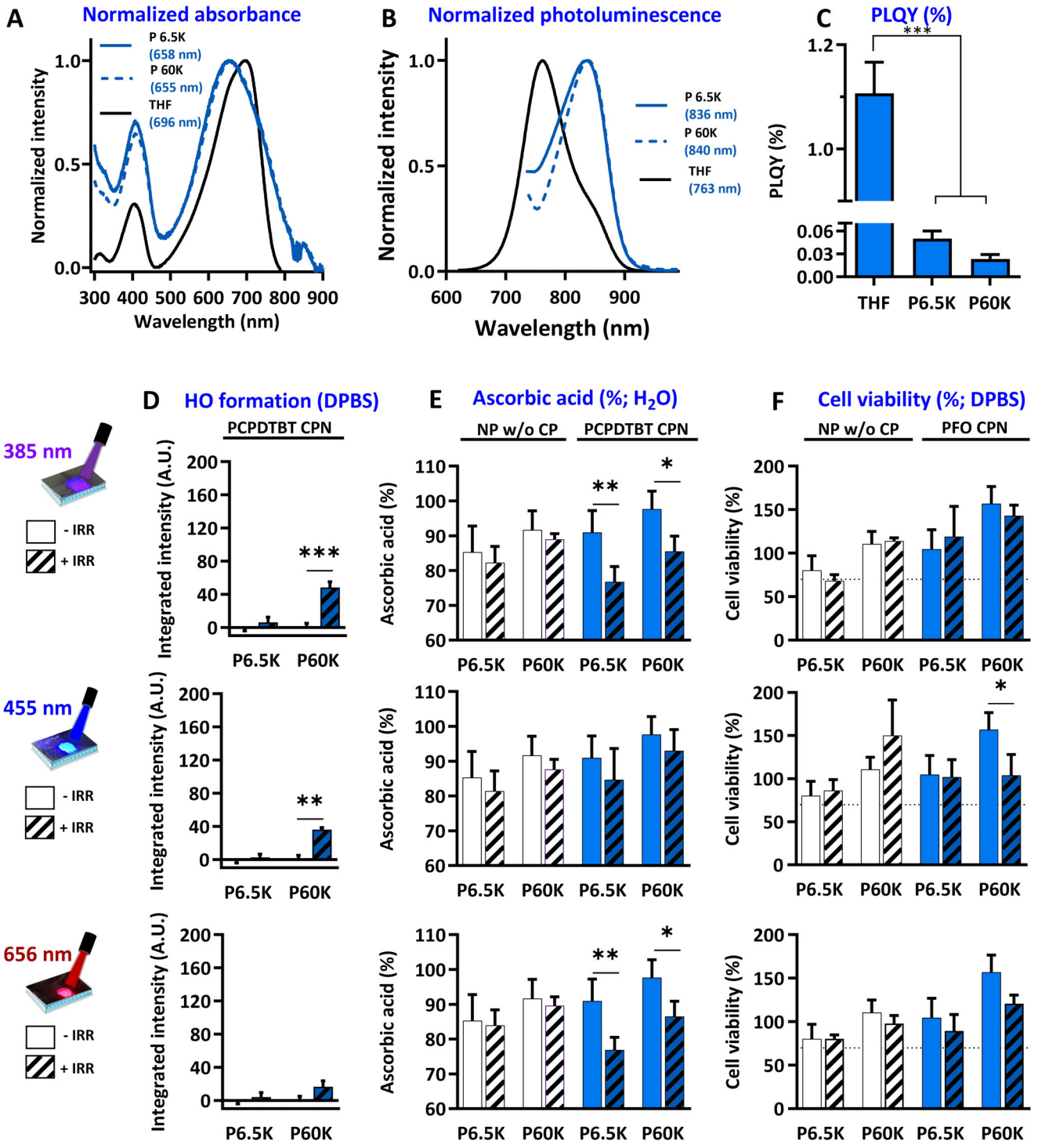

Figure 7. Optical attributes, ROS generation, and phototoxicity of PCPDTBT CPNs. A) Absorbance spectrum, B) emission spectrum, C) PLQY%, D) ROS generation/release in DPBS (30 μg mL^{-1}) measured by EPR, E) ROS generation/release as measured by AA depletion, and F) phototoxicity in 3T3 fibroblasts. (A,B) Spectra are representative of at least $n = 3$ individual samples. (C) Values represent the mean ± standard deviation from $n = 3$ CPN batches, whereas phototoxicity data represent the mean ± standard deviation from $n = 3$ CPN batches tested on three cell passage numbers. *($p < 0.05$), **($p < 0.01$) indicate significant difference.

© 2024 The Author(s). Advanced Therapeutics published by Wiley-VCH GmbH

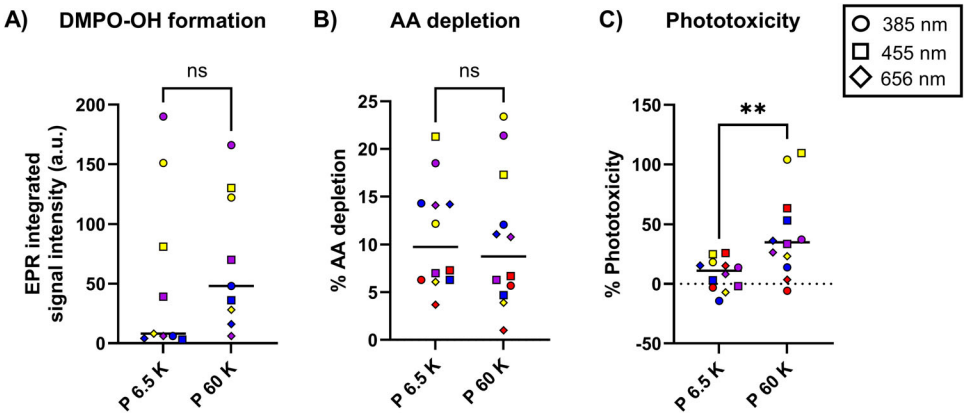

Figure 8. Comparison in A) DMPO-OH formation, B) AA depletion (%), and C) phototoxicity (%) between CPNs with P6.5k and P60k PEG–PLGA matrices following irradiation at 385, 455, and 656 nm. Values depicted represent the mean values from each group. Statistical comparison: unpaired Student's *t*-test; $^{**}p < 0.01$.

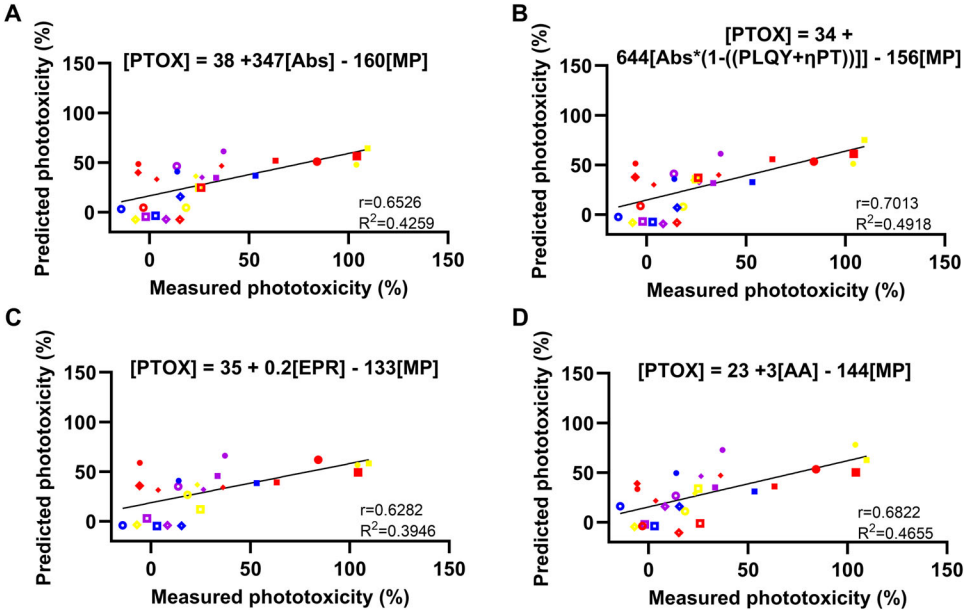

Figure 9. Single parameter correlations between phototoxicity (dependent variable) and A) absorption at all three wavelengths, B) Abs*(1-(PLQY+ ηPT), C) EPR signal intensity, and D) AA depletion (%). Values depicted represent the mean values from each group. Multivariate regression analysis was also performed for phototoxicity results (dependent variable) using the molar concentration of the matrix polymer as one independent variable and the following parameters as the second independent variable: E) absorption at all three wavelengths, F) Abs*(1-(PLQY+ ηPT), G) EPR signal intensity, and H) AA depletion (%). Input values for each model are provided in the Supporting Information. Circles, squares, and diamonds represent samples irradiated at 385, 455, and 656 nm, respectively. Open symbols = P6.5k; closed symbols = P60k, open symbols with dots in the middle = CN-PPV 100%.

to the phototoxicity results. In the single parameter regression analysis (see Supporting Information), the absorbance (expressed as the baseline subtracted peak absolute peak height at 385, 455 or 656 nm), EPR signal intensity and % of ascorbic acid depletion (AA%) were plotted against the % phototoxicity and the Pearson correlation coefficient determined. A further independent variable describing the optical behavior of the systems was calculated by multiplying the peak absorption at each wavelength with a factor that represents energy loss in the form of fluorescence and thermal relaxation (i.e., Abs*(1-(PLQY + ηPT)). As expected, correlation of single parameters with the phototoxicity yielded low Pearson correlation coefficients ($r < 0.4$) and coefficient of determination values ($R^2 < 0.16$).

Addition of the molar concentration of the matrix polymer as a second independent variable improved the models substantially (Figure 9A–D), with increases in the multiple correlation coefficients (r) and the coefficients of multiple determination (R^2). In the multivariate regression analysis, the model including the variable, Abs*(1-(PLQY + ηPT) combined with the molar content of the matrix polymer provided the best description of the phototoxicity data ($r = 0.7013$; $R^2 = 0.4918$). This is indicates that the CP optical properties and choice of matrix are highly influential in determining the phototoxicity regardless of the mechanism of

© 2024 The Author(s). Advanced Therapeutics published by Wiley-VCH GmbH

toxicity (i.e., mediated via type I or II ROS production or photothermal effects).

As can be observed in Figure 9, there are further unknown variables, which will contribute to the phototoxicity results measured here. The data set generated in this study, especially the behavior of the PFO CPNs (with high EPR signals but low levels of biological damage) point toward the possibility that different CPs may produce different ROS species. As discussed by Murphy et al., the identification of individual ROS species with the current techniques can be technically complex,[39] even more so, in the case of CPN, whose inherent fluorescence may interfere with the ROS detection method. EPR, despite its reported low sensitivity, may be the most promising technique for more in-depth studies of ROS generation by using a combination of different spin trapping molecules.[36]

3. Conclusions

The ability of CPs to generate type I and II ROS upon irradiation at different wavelengths is a complex process dependent upon multiple variables including absorbance properties, fluorescence emission, thermal relaxation, intersystem crossing, and phosphorescence. Further, the internal nanoparticle structure, as well as the presence of a matrix polymer or surfactant surface stabilizer, has also been shown to influence ROS production or release into the bulk medium. This study demonstrates that both the CP photophysical properties and the molar content of the PEG–PLGA matrix polymer are major factors influencing CPN phototoxicity, even under conditions of off-target irradiation. The study results highlight that CPN excipients, such as surfactants or matrix polymers, which are required for colloidal stability, can act as ROS scavengers, thereby negatively impacted PDT performance. Further, the results highlight that CP phototoxicity may also occur across the UV/vis spectrum, an insight useful for the design of clinical safety testing studies and off-target effects.

4. Experimental Section

Materials: Poly[2,6-(4,4-bis-(2-ethylhexyl)-4H-cyclopenta[2,1-b;3,4-b]dithiophene)-alt-4,7(2,1,3-benzothiadiazole)] (PCPDTBT), poly(2,5-di(hexyloxy) cyanoterephthalylidene) (CN-PPV), poly[(9,9-di-n-octylfluorenyl-2,7-diyl)-alt-(benzo[2,1,3]thiadiazol-4,8-diyl)] (F8BT), poly(9,9-di-n-octylfluorenyl-2,7-diyl) (PFO), dimethyl sulfoxide (DMSO), TritonTM X-100 (4-(1,1,3,3-Tetramethylbutyl) phenyl-polyethylene glycol (TX), Thiazolyl Blue Tetrazolium Bromide (MTT), and two PEG–PLGA copolymers, $PEG_{2\ kDa}$–$PLGA_{4.5\ kDa}$ (lactide:glycolide ratio of 65:35), and $PEG_{5\ kDa}$–$PLGA_{55\ kDa}$ (lactide:glycolide ratio of 50:50) were purchased from Sigma-Aldrich (Darmstadt, Germany). The spin trap 5,5-dimethyl-1-pyrrolin-N-oxid (DMPO) was purchased from tebu-bio GmbH (Offenbach am Main, Germany). All other chemical reagents used in the study were of analytical reagent grade.

Conjugated Polymer Nanoparticles (CPNs)—Preparation: CPNs were prepared by bulk nanoprecipitation.[20,21] Briefly, a CP stock solution (0.5 mg mL^{-1}) and a PEG–PLGA stock solution (50 mg mL^{-1}) were prepared separately in THF. An organic phase solution containing CP (0.5 mg) and PEG–PLGA (10 mg) was then prepared by mixing 1 mL of CP stock solution with 200 µL of the PEG–PLGA stock solution. Subsequently, 1 mL of the organic phase solution was added dropwise to 5 mL water at room temperature and stirred for up to 12 h to allow complete evaporation of the solvent. The volume of water lost due to evaporation was replaced. Corresponding formulations containing 100% PEG–PLGA or 100% CN-PPV were prepared under the same conditions as controls. Three replicate batches of each formulation were produced, filtered (0.22 µm CA filter) and stored at 4 °C (Figure S1, Supporting Information). The resultant CPN suspensions had a final concentration of ≈2 mg mL^{-1} of PEG–PLGA with a theoretical loading dose of 100 µg CP mL^{-1}, and 2.1 mg mL^{-1} of total solids.

Particle Size and Zeta Potential: Hydrodynamic diameters and zeta potential were assessed by dynamic light scattering and Laser-Doppler anemometry, respectively, using a Zetasizer Nano ZS (Malvern Instruments Ltd., Worcestershire, UK) with a detection angle of 173° and a helium-neon laser operating at 633 nm. All measurements were performed in triplicate at 25 °C after appropriate dilution of freshly prepared samples in filtered (0.22 µm CA filter) distilled water or 10 mM NaCl solution for zeta potential measurements. The size analysis was performed at 50 µg mL^{-1} total solids concentration. Water was chosen as a dispersant with a viscosity of 0.8872 cP at 25 °C and an RI of 1.330. Particle refractive index was matched to PEG–PLGA (1.330). The zeta potential was measured after sample dilution to 20 µg mL^{-1} in standard electrophoresis cuvettes (DTS1070, Malvern Instruments GmbH).

Cell Uptake: An immortalized mouse fibroblast cell line, NIH/3T3 cells (passage numbers 5–18; ATCC, Manassas, USA), derived from BALB/c mice (CRL1658), was chosen for the uptake and phototoxicity studies in accordance with the OECD In Vitro 3T3 NRU Phototoxicity Test guideline.[31] Cells were cultured in a humidified atmosphere of 5% CO_2 at 37 °C. Culture media consisted of high glucose Dulbecco's modified Eagle's medium supplemented with 10% fetal calf serum, and 1% streptomycin and penicillin. Cells were seeded in 96-well plates at a density of 2 × 104 cells per well and incubated at 37 °C for 24 h. For uptake studies, cells were washed with 150 µL warm DPBS, then incubated for 1 h at 37 °C with CPNs (20 µg CP cm^{-2}; 30 µg CP mL^{-1}). Following cell lysis, CPN absorbance was measured at the optimum CPN absorbance wavelengths (Table 1). Calibration curves ($n = 3$) were prepared for each CPN formulation and limit of detection/quantification values established (Table S1, Supporting Information).

Optical Properties: Absorption spectra of CPs dissolved in THF (99%; 3 µg CP mL^{-1}) or CPN (theoretical concentration 3 µg mL^{-1}) were acquired at room temperature using a FluoroMax-4 (HORIBA Instruments Inc.) scanning from 300 to 950 nm, with an integration time of 1 s, increments of 0.5 nm, and an excitation slit width of 2 nm. Molar extinction coefficients of the CPN were estimated based on the absorbance at different CPN concentrations (see the Supporting Information) and median reported molecular weight (MW) of the CP provided by the manufacturer (Table 1). Photoluminescence spectra were acquired with the FluoroMax-4 (HORIBA Instruments Inc.) using the settings listed in Table S2 of the Supporting Information. Integration time of 1 s and increments of 0.5 nm (THF) or 1 nm (CPNs) were used. Normalized curves were prepared by dividing each value by the maximum value.

PLQY values (%) were determined with the FluoroMax-4 using the PTI K-Sphere in the sample compartment. Three replicate batches were prepared for each CP in THF with a final concentration of 1 µg CP mL^{-1} (absorbance was < 0.1 in all cases). Slits on the excitation and emission monochromators were set to 3 nm with an integration time of 1 s in increments of 0.5 nm. All measurements above described were performed at room temperature using a 10 mm quartz cuvette.

ROS Production and Detection—Irradiation: Three precision LED spotlights (BLS-PLS-0385-030-04-S, BLS-PLS-0455-030-S, and BLS-PLS-0656-030-03-S from Mightex) with wavelengths at 385, 455, and 656 nm were used to irradiate samples in well plates (+IRR), both in acellular and cellular assays. During each experiment, the spotlight was positioned 12.3 cm above the plate and with the LED source Controller (Mightex BLS-1000-2) set at maximum power (Figure S4, Supporting Information). Following the incubation of 1 h, the +IRR plate was exposed to an irradiation dose of 5 J cm^{-2} for an irradiation time dependent on the spotlight used (Equation (1)). The −IRR plate was placed at room temperature in the dark during the duration of irradiation procedure to maintain the same environ-

© 2024 The Author(s). Advanced Therapeutics published by Wiley-VCH GmbH

mental conditions for both plates. The duration of irradiation for the light dose (LD) was calculated according to (Equation (1))

$$\text{Time [min]} = \frac{(\text{LD} \cdot A \cdot 1000)}{(\text{OP} \cdot 60)} \quad (1)$$

where LD is the light dose = 5 J cm^{-2} (OECD Test Guideline No. 432),[31] A is the area of illumination (10.7 cm^2), and OP is the total optical power of the LED spotlight (250, 150, and 180 mW for the 385, 455, and 656 nm spotlights, respectively). According to Equation (1), irradiation times of 4, 6, and 5 min were required for the 385, 455, and 656 nm spotlights, respectively.

Electron Paramagnetic Resonance (EPR): The spin trap DMPO was used to detect short-lived radicals (e.g., OH· or OOH·) generated after the irradiation of selected samples. EPR studies were performed on a single batch of CPN formulations at room temperature. Briefly, a 300 µL volume of each CPN suspension diluted in DPBS (final concentration of 30 µg CP mL^{-1}) was mixed with 3 µL DMPO (30 µL mL^{-1} as recommended by the manufacturer Dojinjo) in a 24 well plate. The sample was then irradiated with one of the three different precision LED spotlights (λ_{ex} = 385, 455, and 656 nm) and the same irradiation times used for the phototoxicity and AA depletion assays (i.e., 4, 6, and 5 min, respectively) were applied. The irradiated samples were subsequently filled into 50 µL capillaries, closed with sealing compound and measured immediately in a MiniScope MS 200 spectrometer (Magnettech, Berlin, Germany). Spectra were acquired by using the following settings: B0 = 336.5 mT, sweep = 7 mT, measurement time = 180 s, modulation amplitude = 0.12 mT. The recorded spectra were processed, fitted, and double integrated with easyspin 8. The averages and standard deviations were calculated from three measurements with OriginPro 2019 (OrigiLab, Northampton, USA). Spectra of the media used in this study, i.e., DPBS and deionized filtered water (0.22 µm CA filter), with DMPO (30 µL mL^{-1}) and with and without irradiation were also acquired to assess the influence of medium on the signal (Figure S2, Supporting Information). The pure DPBS integrals were subtracted from the data to correct for intensities from the noise and medium. For more detailed information, readers are requested to consult the Supporting Information.

Ascorbic Acid (AA) Depletion: The AA depletion assay was performed according to the approach reported by Yang et al.[37] Briefly, in each well of a 12-well plate 1.5 mL of each CPN suspension was diluted with deionized filtered water to 30 µg CP mL^{-1} with and without 187.5 µL AA stock solution (2 mM). The wells were irradiated with one of the three different precision LED spotlights (λ_{ex} = 385, 455, and 656 nm) for the same irradiation times used in the phototoxicity assay (i.e., 4, 6, and 5 min, respectively). Plates without irradiation (−IRR) were also prepared and processed in the same way. Following incubation for 10 min at 37 °C, samples were centrifuged at 2100 rcf for 10 min in Amicon Ultra-15 Centrifugal Filter units (100 kDa MWCO). The AA absorbance of the filtrate was measured at 265 nm and the decrease in absorbance was calculated as a percentage of the negative control (distilled water), which was processed in the same way as the CPN samples. Hydrogen peroxide solutions (4–128 mM) were chosen as references (Figure S3, Supporting Information). To assess the effect of dispersion medium on the AA depletion results, the same assay was performed using CN-PPV 100% and F8BT CPN formulations diluted in DPBS (30 µg CP mL^{-1}). DPBS was used as medium in the phototoxicity assay and the EPR experiments.

Cellular Phototoxicity: Two identical 96-well plates were prepared for each passage number/replicate: one for irradiation (+IRR) and a non-irradiated (−IRR) control plate. Cells were washed with 150 µL warm DPBS, then incubated for 1 h at 37 °C with CPN or blank PEG–PLGA formulations (20 µg CP or 0.4 mg PEG–PLGA cm^{-2}). Negative controls were incubated with DPBS containing an equal volume of distilled water as in the CPN samples. A 1% Triton-X solution in DPBS (TX) was used as a positive control for cytotoxicity (data not shown). After irradiation, the treatment medium was removed, cells were washed with 150 µL DPBS, and incubated 24 h at 37 °C with 200 µL cell culture medium prior to the cell viability assessment using the MTT tetrazolium reduction assay. Briefly, following irradiation and the subsequent 24 h incubation, MTT solution was added to selected wells in both plates (+IRR/−IRR) to achieve a final concentration of 0.5 mg mL^{-1}.[42] The plates were incubated for 3 h, the supernatant removed, 100 µL DMSO was added to each well and the plates were shaken for 5 min. Absorbance was measured without the plate lid at λ = 570 nm (Epoch 2 UV–Vis spectrophotometer; Biotek Instruments Inc. Bad Friedrichshall, Germany). Absorbance of wells containing CPN but without MTT was subtracted from each sample and the cell viability was calculated as a percentage of the untreated control wells. Assays were performed in triplicate with different cellular passage numbers (in compliance with ISO 10993-5)[43] and n = 3 CPN batches.

Statistical Analysis: Prism 10.0 software (GraphPad Prism, CA, USA) was used to perform statistical analyses (one-way and two-way ANOVA followed by Tukey and Bonferroni post-test, and unpaired Student's t-test). Values were considered significant when *($p < 0.05$), **$p < 0.01$, ***($p < 0.001$), and ****($p < 0.0001$).

Supporting Information

Supporting Information is available from the Wiley Online Library or from the author.

Acknowledgements

P.M. and M.-L.T. contributed equally to this work.

Conflict of Interest

The authors declare no conflict of interest.

Data Availability Statement

The data that support the findings of this study are openly available in Zenodo at 10.5281/zenodo.11110289, reference number 1.

Keywords

π-conjugated polymer, photodynamic therapy, phototoxicity, reactive oxygen species

Received: May 3, 2024
Revised: November 11, 2024
Published online:

[1] B. Liu, in *Conjugated Polymers for Biological and Biomedical Applications*, Wiley-VCH, Weinheim, Germany **2018**, p. 424.
[2] M. Zhao, E. Leggett, S. Bourke, S. Poursanidou, S. Carter-Searjeant, S. Po, M. Palma do Carmo, L. A. Dailey, P. Manning, S. G. Ryan, L. Urbano, M. A. Green, A. Rakovich, *ACS Nano* **2021**, *15*, 8790.
[3] G. Feng, Y. Fang, J. Liu, J. Geng, D. Ding, B. Liu, *Small* **2017**, *13*, 1602807.
[4] X. Wang, Z. Geng, H. Cong, Y. Shen, B. Yu, *ChemBioChem* **2019**, *20*, 1628.
[5] H. Shi, Y. Wang, X. Huang, P. Liang, Y. Tang, Y. Zhang, N. Fu, W. Huang, X. Dong, *J. Mater. Chem. B* **2018**, *6*, 7402.
[6] J. Li, J. Rao, K. Pu, *Biomaterials* **2018**, *155*, 217.
[7] J. M. Dąbrowski, *Adv. Inorg. Chem.* **2017**, *70*, 343.
[8] D. Tuncel, *Nanoscale Adv.* **2019**, *1*, 19.
[9] K. Li, B. Liu, *J. Mater. Chem.* **2012**, *22*, 1257.

© 2024 The Author(s). Advanced Therapeutics published by Wiley-VCH GmbH

[10] C. Zhu, L. Liu, Q. Yang, F. Lv, S. Wang, *Chem. Rev.* **2012**, *112*, 4687.
[11] Y.-H. Chan, P.-J. Wu, *Part. Part. Syst. Charact.* **2015**, *32*, 11.
[12] J. R. Lakowicz, *Principles of Fluorescence Spectroscopy*, 3rd ed., Springer, New York **2006**.
[13] Z. Meng, W. Hou, H. Zhou, L. Zhou, H. Chen, C. Wu, *Macromol. Rapid Commun.* **2018**, *39*, 1700614.
[14] H. Sun, F. T. Lv, L. B. Liu, Q. Gu, S. Wang, *Adv. Ther.* **2018**, *1*, 1800057.
[15] A. Blacha-Grzechnik, *Materials* **2021**, *14*, 1098.
[16] A. Wilm, M. Berneburg, Z. Hautkrankh, *JDDG* **2015**, *13*, 7.
[17] E. Gonzalez, S. Gonzalez, *J. Am. Acad. Dermatol.* **1996**, *35*, 871.
[18] P. Modicano, P. R. Neumann, M. Schuller, J. Holthof, F. L. Kyrilis, F. Hamdi, P. L. Kastritis, K. Mader, L. Ann Dailey, *Eur. J. Pharm. Biopharm.* **2020**, *154*, 297.
[19] D. L. Crossley, L. Urbano, R. Neumann, S. Bourke, J. Jones, L. A. Dailey, M. Green, M. J. Humphries, S. M. King, M. L. Turner, M. J. Ingleson, *ACS Appl. Mater. Interfaces* **2017**, *9*, 28243.
[20] T. F. Abelha, T. W. Phillips, J. H. Bannock, A. M. Nightingale, C. A. Dreiss, E. Kemal, L. Urbano, J. C. deMello, M. Green, L. A. Dailey, *Nanoscale* **2017**, *9*, 2009.
[21] E. Kemal, T. F. Abelha, L. Urbano, R. Peters, D. M. Owen, P. Howes, M. Green, L. A. Dailey, *RSC Adv.* **2017**, *7*, 15255.
[22] P. R. Neumann, D. L. Crossley, M. Turner, M. Ingleson, M. Green, J. Rao, L. A. Dailey, *ACS Appl. Mater. Interfaces* **2019**, *11*, 46525.
[23] T. F. Abelha, P. R. Neumann, J. Holthof, C. A. Dreiss, C. Alexander, M. Green, L. A. Dailey, *J. Mater. Chem. B* **2019**, *7*, 5115.
[24] P. R. Neumann, F. Erdmann, J. Holthof, G. Hadrich, M. Green, J. Rao, L. A. Dailey, *Adv. Healthcare Mater.* **2021**, *10*, 2001089.
[25] E. Kemal, R. Peters, S. Bourke, S. Fairclough, P. Bergstrom-Mann, D. M. Owen, L. Sandiford, L. A. Dailey, M. Green, *Photochem. Photobiol. Sci.* **2018**, *17*, 718.
[26] B. Romberg, W. E. Hennink, G. Storm, *Pharm. Res.* **2008**, *25*, 55.
[27] T. F. Abelha, J. Calvo-Castro, S. M. Lima, J. R. Silva, L. H. D. Andrade, J. C. D. Mello, C. A. Dreiss, M. Green, L. A. Dailey, *ACS Appl. Polym. Mater.* **2022**, *4*, 6219.
[28] T. D. Pham, S. J. Jung, C. M. Oh, J. K. Yang, D. Lee, A. Kidanemariam, A. Muhammad, S. Kim, T. J. Shin, J. H. Park, I. W. Hwang, J. Park, *Macromolecules* **2023**, *56*, 311.
[29] S. I. H. Abdi, J. Y. Choi, H. C. Lau, J. O. Lim, *Tissue Eng. Regener. Med.* **2013**, *10*, 131.
[30] E. Boix-Garriga, P. Acedo, A. Casadó, A. Villanueva, J. C. Stockert, M. Cañete, M. Mora, M. L. Sagristá, S. Nonell, *Nanotechnology* **2015**, *26*, 365104.
[31] *Test No. 432: In Vitro 3T3 NRU Phototoxicity Test*, OECD, France **2019**, p. 20.
[32] P. L. C. Feyen, B. F. E. Matarese, L. Urbano, T. F. Abelha, H. Rahmoune, M. Green, L. A. Dailey, J. C. de Mello, F. Benfenati, *Front. Bioeng. Biotechnol.* **2022**, *10*, 932877.
[33] Y. Li, M. Kröger, W. K. Liu, *Biomaterials* **2014**, *35*, 8467.
[34] R. Weissleder, M. Nahrendorf, M. J. Pittet, *Nat. Mater.* **2014**, *13*, 125.
[35] B. Halliwell, *FEBS Lett.* **2003**, *540*, 3.
[36] J.-L. Clément, P. Tordo, in *Electron Paramagnetic Resonance*, Vol. *20* (Eds: B. C. Gilbert, M. B. Davies, D. M. Murphy), Royal Society of Chemistry, Cambridge **2007**, p. 29.
[37] A. Yang, A. Jedynska, B. Hellack, I. Rooter, G. Hoek, B. Brunekreef, T. A. J. Kuhlbusch, F. R. Cassee, N. A. H. Janssen, *Atmos. Environ.* **2014**, *83*, 35.
[38] C. Nishizawa, K. Takeshita, J. Ueda, M. Mizuno, K. T. Suzuki, T. Ozawa, *Free Radical Res.* **2004**, *38*, 385.
[39] M. P. Murphy, H. Bayir, V. Belousov, C. J. Chang, K. J. A. Davies, M. J. Davies, T. P. Dick, T. Finkel, H. J. Forman, Y. Janssen-Heininger, D. Gems, V. E. Kagan, B. Kalyanaraman, N. G. Larsson, G. L. Milne, T. Nyström, H. E. Poulsen, R. Radi, H. Van Remmen, P. T. Schumacker, P. J. Thornalley, S. Toyokuni, C. C. Winterbourn, H. Yin, B. Halliwell, *Nat. Metab.* **2022**, *4*, 651.
[40] A. Kumar, L. A. Dailey, M. Swedrowska, R. Siow, G. E. Mann, G. Vizcay-Barrena, M. Arno, I. S. Mudway, B. Forbes, *FEBS Lett.* **2016**, *590*, 258.
[41] J. J. Mittag, M.-L. Trutschel, H. Kruschwitz, K. Mäder, J. Buske, P. Garidel, *Int. J. Pharm.: X* **2022**, *4*, 100123.
[42] T. L. Riss, R. A. Moravec, A. L. Niles, S. Duellman, H. A. Benink, T. J. Worzella, L. Minor, Eli Lilly & Company and the National Center for Advancing Translational Sciences **2004**, (Eds: S. Markossian, A. Grossman, M. Arkin), available from: https://www.ncbi.nlm.nih.gov/books/NBK144065/ (accessed: October **2024**).
[43] International Standard Organization–ISO (ISO-10993-5), *Biological Evaluation of Medical Devices-Part 5: Tests for In Vitro Cytotoxicity*, International Standard Organization, Geneva **2009**.

© 2024 The Author(s). Advanced Therapeutics published by Wiley-VCH GmbH